

Thermoelastic Properties of Ringwoodite (Fe_xMg_{1-x})₂SiO₄: Its Relationship to the 520 km Seismic Discontinuity.

Maribel Núñez Valdez^{a,*}, Zhongqing Wu^{b,c}, Yonggang G. Yu^c, Justin
Revenaugh^d, Renata M. Wentzcovitch^{c,e}

^a*School of Physics and Astronomy, University of Minnesota, Minneapolis, MN 55414, USA*

^b*School of Earth and Space Sciences, University of Science and Technology of China, Hefei, Anhui 230026, China*

^c*Department of Chemical Engineering and Materials Science, University of Minnesota, Minneapolis, MN 55414, USA*

^d*Department of Earth Sciences, University of Minnesota, Minneapolis, MN 55414, USA*

^e*Minnesota Supercomputing Institute, University of Minnesota, Minneapolis, MN 55414, USA*

Abstract

We combine density functional theory (DFT) within the local density approximation (LDA), the quasiharmonic approximation (QHA), and a model vibrational density of states (VDoS) to calculate elastic moduli and sound velocities of γ -(Fe_xMg_{1-x})₂SiO₄ (ringwoodite), the most abundant mineral of the lower Earth's transition zone (TZ). Comparison with experimental values at room-temperature and high pressure or ambient-pressure and high temperature shows good agreement with our first-principles findings. Then, we investigate the contrasts associated with the $\beta \rightarrow \gamma$ -(Fe_xMg_{1-x})₂SiO₄ transformation at pressures and temperatures relevant to the TZ. This information offers clearly defined reference values to advance the understanding

*Corresponding author. Tel.: +1 612 624 2872; fax: +1 612 626 7246
Email address: valdez@physics.umn.edu (Maribel Núñez Valdez)

of the nature of the 520 km seismic discontinuity.

Keywords: first principles, ringwoodite, elasticity, transition zone, 520 km discontinuity

1. Introduction

Wadsleyite (β -phase) and ringwoodite (γ -phase) are the high-pressure polymorphs of olivine (α -phase), $(\text{Fe}_x, \text{Mg}_{1-x})_2\text{SiO}_4$. These minerals are the main constituents of the Earth's upper mantle (UM) (Ringwood, 1975; Putnis, 1992) and transition zone (TZ) (Irifune and Ringwood, 1987). Under pressure, the transformation from olivine to wadsleyite happens at ~ 13.5 GPa and from wadsleyite to ringwoodite at ~ 18 GPa near 1600 K (Katsura and Ito, 1989; Akaogi et al., 1989). These transformations are associated with two major discontinuities in seismic velocities in the Earth's interior at about 410 km and 520 km depth, respectively (Revenaugh and Jordan, 1991). While the first discontinuity is a well characterized and sharp feature in seismic data, the second varies considerably with location.

Experimental and computational approaches have been used to study properties of these minerals at *in situ* conditions and their relationship with seismic discontinuities. Mg-end member and Fe-bearing α -phases have been widely investigated at simultaneous high pressure and temperature. Computational results and experimental data on elastic properties and sound velocities seem to be consistent with seismic measurements (see e.g. Núñez Valdez et al., 2010; Stackhouse et al., 2010; Li and Liebermann, 2007, and references therein). On the other hand, even though great efforts have been made to obtain measurements of elastic properties and wave velocities of Fe-free and

22 Fe-bearing wadsleyite and ringwoodite under high temperature and pres-
 23 sure using either ultrasonic or Brillouin scattering techniques (Li et al., 1996;
 24 Zha et al., 1997; Isaak et al., 2007; Sinogeikin et al., 1998; Li and Liebermann,
 25 2000; Liu et al., 2009; Mayama et al., 2004; Isaak et al., 2010; Li, 2003; Higo et al.,
 26 2006; Weidner et al., 1984; Sinogeikin et al., 2003; Jackson et al., 2000; Mayama et al.,
 27 2005), results are still limited. Therefore large extrapolations from room con-
 28 ditions to conditions of the TZ are often used.

29 First principles calculations employing the quasiharmonic approximation
 30 (QHA), valid up to about two thirds of the melting temperature, or molecular
 31 dynamics (MD) methods, valid near and above melting temperatures, com-
 32 plement each other and are used to obtain elastic moduli under high-pressure-
 33 temperature conditions. Calculations of elastic constants using the QHA,
 34 though computationally less demanding than MD, still required calculations
 35 of vibrational density of states (VDoS) for each strained atomic configura-
 36 tion at several pressures, that is, about 1000 parallel jobs (Da Silveira et al.,
 37 2008, 2011).

38 In this paper we use the analytical and computational approach by Wu and Wentzcovitch
 39 (2011) and tested on periclase-MgO, α -Mg₂SiO₄, and more recently on
 40 β -(Fe_xMg_{1-x})₂SiO₄ (Núñez Valdez et al., 2012), to calculate bulk (K) and
 41 shear (G) moduli and sound velocities of the γ -(Fe_xMg_{1-x})₂SiO₄ phase.
 42 This method uses only static elastic constants and phonon density of states
 43 for unstrained configurations, therefore reducing the amount of computa-
 44 tional time and resources by one to two orders of magnitude. We then ad-
 45 dress contrasts across the $\beta \rightarrow \gamma$ -(Fe_xMg_{1-x})₂SiO₄ transition near conditions
 46 of the 520 km seismic discontinuity.

2. Methodology

2.1. Computational Details

Calculations based on Density Functional Theory (DFT) (Hohenberg and Kohn, 1964; Kohn and Sham, 1965) were performed using the local density approximation (LDA) (Ceperley and Alder, 1980). Ultrasoft pseudopotentials generated by the Vanderbilt method (Vanderbilt, 1990) were used to describe Fe, Si, and O. A norm-conserving pseudopotential generated by the von Car method was used for Mg. Further details about these pseudopotentials are given in (Núñez Valdez et al., 2011). Equilibrium structures of ringwoodite (28 atoms/cell) at arbitrary pressures were found using the variable cell-shape damped molecular dynamics approach (Wentzcovitch, 1991; Wentzcovitch et al., 1993) as implemented in the quantum-ESPRESSO (QE) code (Giannozzi et al., 2009). The plane-wave kinetic energy cutoff used was 40 Ry and for the charge density 160 Ry. The \mathbf{k} -point sampling of the charge density was determined on a $2 \times 2 \times 2$ Monkhorst-Pack grid of the Brillouin Zone (BZ) shifted by $(\frac{1}{2}\frac{1}{2}\frac{1}{2})$ from the origin. These parameters correspond to having interatomic forces smaller than 10^{-4} Ry/a.u. and pressure convergence within 0.5 GPa. Dynamical matrices were obtained using density functional perturbation theory (DFPT) (Baroni et al., 2001) via QE. At each pressure, a dynamical matrix was calculated on a $2 \times 2 \times 2$ \mathbf{q} -point mesh for one atomic configuration only. In principle about 10 other configurations should be used as well, but here we are more interested in frequencies with strain and the current approximation seems to be sufficiently accurate. Force constants were extracted and interpolated to a $12 \times 12 \times 12$ regular \mathbf{q} -point mesh to produce VDoS.

72 2.2. High-Temperature-Pressure Elastic Theory

73 Exploiting the information about the strain and volume dependence of
 74 phonon frequencies, we determine the thermal contribution to the Helmholtz
 75 free energy F within the QHA (Wallace, 1972), that is,

$$F(e, V, T) = U_{st}(e, V) + \frac{1}{2} \sum_{\mathbf{q}, m} \hbar \omega_{\mathbf{q}, m}(e, V) + \\ + k_B T \sum_{\mathbf{q}, m} \ln \left\{ 1 - \exp \left[-\frac{\hbar \omega_{\mathbf{q}, m}(e, V)}{k_B T} \right] \right\}, \quad (1)$$

76 where \mathbf{q} is the phonon wave vector, m is the normal mode index, T is tem-
 77 perature, U_{st} is the static internal energy at equilibrium volume V under
 78 isotropic pressure P and infinitesimal strain e , \hbar and k_B are Planck and
 79 Boltzmann constants, respectively. Isothermal elastic constants are given by

$$C_{ijkl}^T = \left[\frac{\partial^2 G(P, T)}{\partial e_{ij} \partial e_{kl}} \right]_P, \quad (2)$$

80 with $G = F + PV$, the Gibbs energy, and $i, j, k, l = 1, \dots, 3$. To convert to
 81 adiabatic elastic constants, one uses the relationship:

$$C_{ijkl}^S = C_{ijkl}^T + \frac{T}{V C_V} \frac{\partial S}{\partial e_{ij}} \frac{\partial S}{\partial e_{kl}} \delta_{ij} \delta_{kl}, \quad (3)$$

82 where C_V is heat capacity at constant volume, and S is entropy. For or-
 83 thorhombic crystals, the non-shear elastic constants of Eq. (2) are:

$$C_{iijj}^T = \left[\frac{\partial^2 F(\mathbf{e}, V, T)}{\partial e_{ii} \partial e_{jj}} \right]_P + (1 - \delta_{ij}) P(V, T), \\ = C_{iijj}^{st}(V) + C_{iijj}^{ph}(V, T), \quad (4)$$

84 while the shear elastic constants are:

$$C_{ijij}^T = C_{ijij}^{st}(V) + C_{ijij}^{ph}(V, T). \quad (5)$$

85 Elastic constants C_{ijj}^{ph} and C_{iji}^{ph} can be expressed as functions of the volume
 86 Grüneisen parameters, $\gamma_{\mathbf{q},m} = -\partial(\ln \omega_{\mathbf{q},m})/\partial(\ln V)$:

$$\frac{d\omega_{\mathbf{q},m}}{\omega_{\mathbf{q},m}} = -\gamma_{\mathbf{q},m} \frac{dV}{V}, \quad (6)$$

87 or the generalization to strain Grüneisen parameters:

$$\frac{\partial \omega_{\mathbf{q},m}}{\omega_{\mathbf{q},m}} = -\gamma_{\mathbf{q},m}^{ij} e_{ij}. \quad (7)$$

88 We have used the Wu-Wentzcovitch method (Wu and Wentzcovitch, 2011)
 89 to compute the thermal contribution to the elastic constants, $C_{ijj}^{ph}(V, T)$.
 90 This method allows the computation of thermal elastic constants without
 91 performing phonon calculations for strained configurations with the approx-
 92 imation that strain and mode Grüneisen parameters have isotropic distribu-
 93 tion, which is equivalent to assuming that thermal pressure is isotropic. This
 94 is a good approximation (Carrier et al., 2007) implicit in the QHA calcula-
 95 tion of thermal pressures.

96 After obtaining VDoS at several volumes by first principles, average
 97 strain Grüneisen parameters were computed at such volumes and interpo-
 98 lated in a fine volume-temperature grid, that was then inverted to a pressure-
 99 temperature grid of 0.1 GPa and 10 K spacings. Static elastic constants
 100 previously computed (Núñez Valdez et al., 2011) were also used.

101 Voigt and Reuss bounds of bulk and shear moduli of orthorhombic crys-
 102 tals at high temperature were calculated using adiabatic elastic constants as

103 (Watt et al., 1976; Watt, 1979):

$$K_V = \frac{1}{9} [C_{11} + C_{22} + C_{33} + 2(C_{12} + C_{13} + C_{23})], \quad (8)$$

$$G_V = \frac{1}{15} [C_{11} + C_{22} + C_{33} + 3(C_{44} + C_{55} + C_{66}) - (C_{12} + C_{13} + C_{23})], \quad (9)$$

$$K_R = D [C_{11} (C_{22} + C_{33} - 2C_{23}) + C_{22} (C_{33} - 2C_{13}) - 2C_{33}C_{12} + C_{12} (2C_{23} - C_{12}) + C_{13} (2C_{12} - C_{13}) + C_{23} (2C_{13} - C_{23})]^{-1}, \quad (10)$$

$$G_R = 15 \{4 [C_{11} (C_{22} + C_{33} + C_{23}) + C_{22} (C_{33} + C_{13}) + C_{33}C_{12} - C_{12} (C_{12} + C_{23}) - C_{13} (C_{13} + C_{12}) - C_{23} (C_{23} + C_{13})] / D + 3(1/C_{44} + 1/C_{55} + 1/C_{66})\}^{-1}, \quad (11)$$

$$D = C_{13} (C_{12}C_{23} - C_{13}C_{22}) + C_{23} (C_{12}C_{13} - C_{23}C_{11}) + C_{33} (C_{11}C_{22} - C_{12}^2). \quad (12)$$

104 With Voight-Reuss-Hill averages of elastic moduli, i.e.,

$$K = \frac{K_V + K_R}{2} \quad \text{and} \quad G = \frac{G_V + G_R}{2}, \quad (13)$$

105 isotropic sound velocities are given by:

$$V_P = \sqrt{\frac{K + \frac{4}{3}G}{\rho}}, \quad V_S = \sqrt{\frac{G}{\rho}}, \quad V_\Phi = \sqrt{\frac{K}{\rho}}, \quad (14)$$

106 where ρ is density, and V_P , V_S , and V_Φ are compressional, shear and bulk
107 velocities, respectively.

108 3. Results

109 We present first-principles results of aggregate properties of Fe-bearing
110 ringwoodite at pressures and temperatures relevant to the TZ. All the ap-

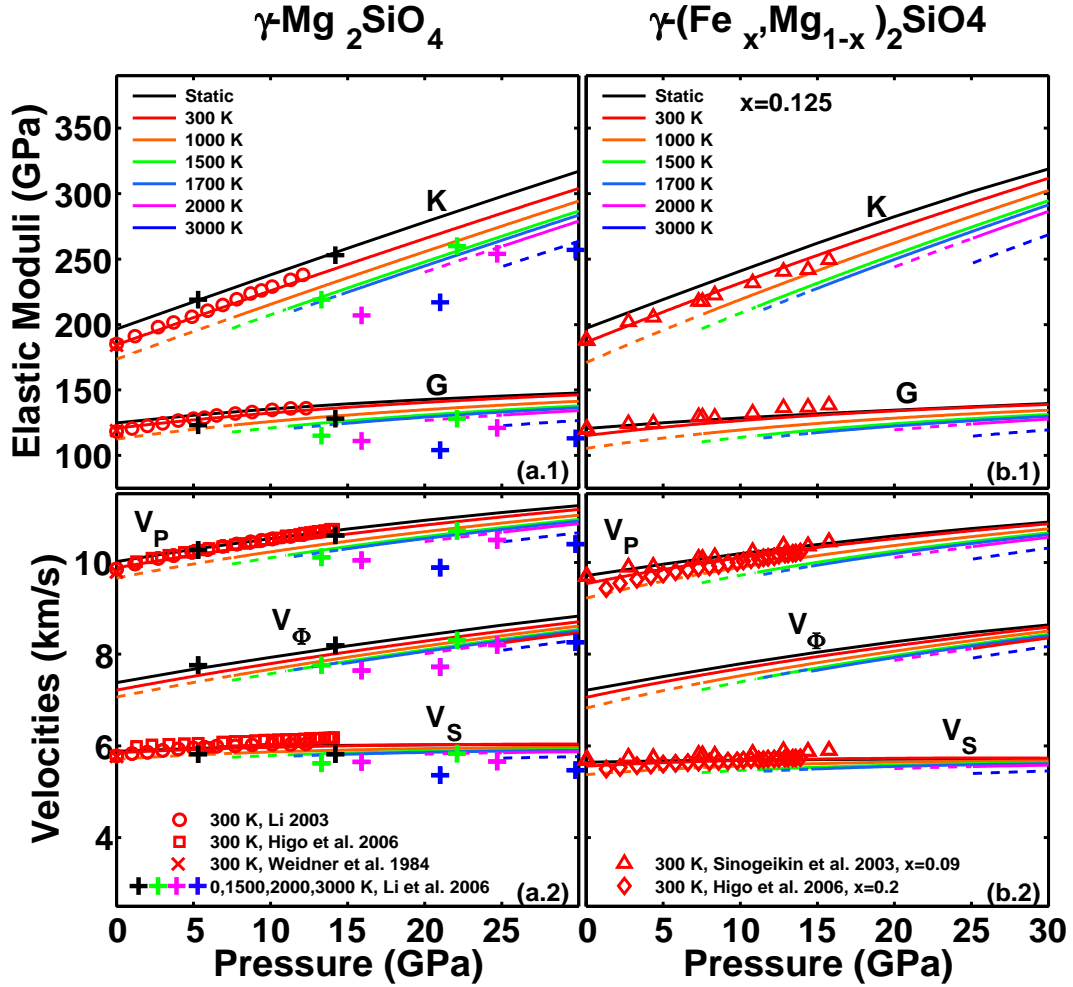


Figure 1: (Color online) Pressure and temperature dependence of bulk modulus (K), shear modulus (G), compressional velocity (V_P), shear velocity (V_S) and bulk velocity (V_Φ) for Fe-free ringwoodite (a,c) and Fe-bearing ringwoodite (b,d). First principles calculations within LDA (solid lines) are compared to available experimental data (symbols). Note, however, that low-pressure-high temperature calculated trends (dash lines) are outside the validity of the QHA.

111 proximations described in the previous section provided an excellent de-
 112 scription of bulk and shear moduli, and sound velocities within the valid
 113 regime of the QHA established for the Fe-free quantities (Yu et al., 2008) for
 114 $\gamma-(\text{Fe}_x\text{Mg}_{1-x})_2\text{SiO}_4$ with $x = 0$ and $x = 0.125$ (see Figs. 1 and 2).

115 In the case of the Mg-end member ringwoodite, K increases more rapidly
 116 than G , as a function of pressure, and decreases faster than G with increas-
 117 ing temperature. At 300 K the agreement between experimental data (Li,
 118 2003; Higo et al., 2006; Weidner et al., 1984) and our DFT-results is truly
 119 excellent for elastic moduli (Fig. 1a), and sound velocities (Fig. 1c). Re-
 120 sults from a molecular dynamics study by Li et al. (2006) also compare well
 121 with our results for K , V_P , and V_Φ within the QHA limits. Our predicted G
 122 and V_S are larger and smaller, respectively, than molecular dynamics values
 123 Li et al. (2006). This difference is primarily caused by the use of the GGA
 124 approximation in the MD simulation. Nevertheless the general agreement
 125 is good and it is the only other source to compare aggregate properties of
 126 $\gamma\text{-Mg}_2\text{SiO}_4$ at high pressures and temperatures. Results of Fe-bearing ring-
 127 woodite as function of pressure are shown in Figs. 1b and 1d. Experimental
 128 data by Sinogeikin et al. (2003) at room temperature and $x = 0.09$ are in
 129 excellent agreement with our 300 K curve, though after 10 GPa our K tends
 130 to be larger, while G tends to be smaller (Fig. 1b). Fe-bearing compres-
 131 sional, shear and bulk velocities are smaller than their Fe-free counterparts
 132 (Fig. 1d). Predictions for $x = 0.125$ fall in between two experimental reports
 133 with iron concentrations of $x = 0.09$ (Sinogeikin et al., 2003) and $x = 0.2$
 134 (Higo et al., 2006). From Fig. 1d one can see that V_P is the most affected by
 135 iron concentration and temperature, while V_S seems to be the least affected

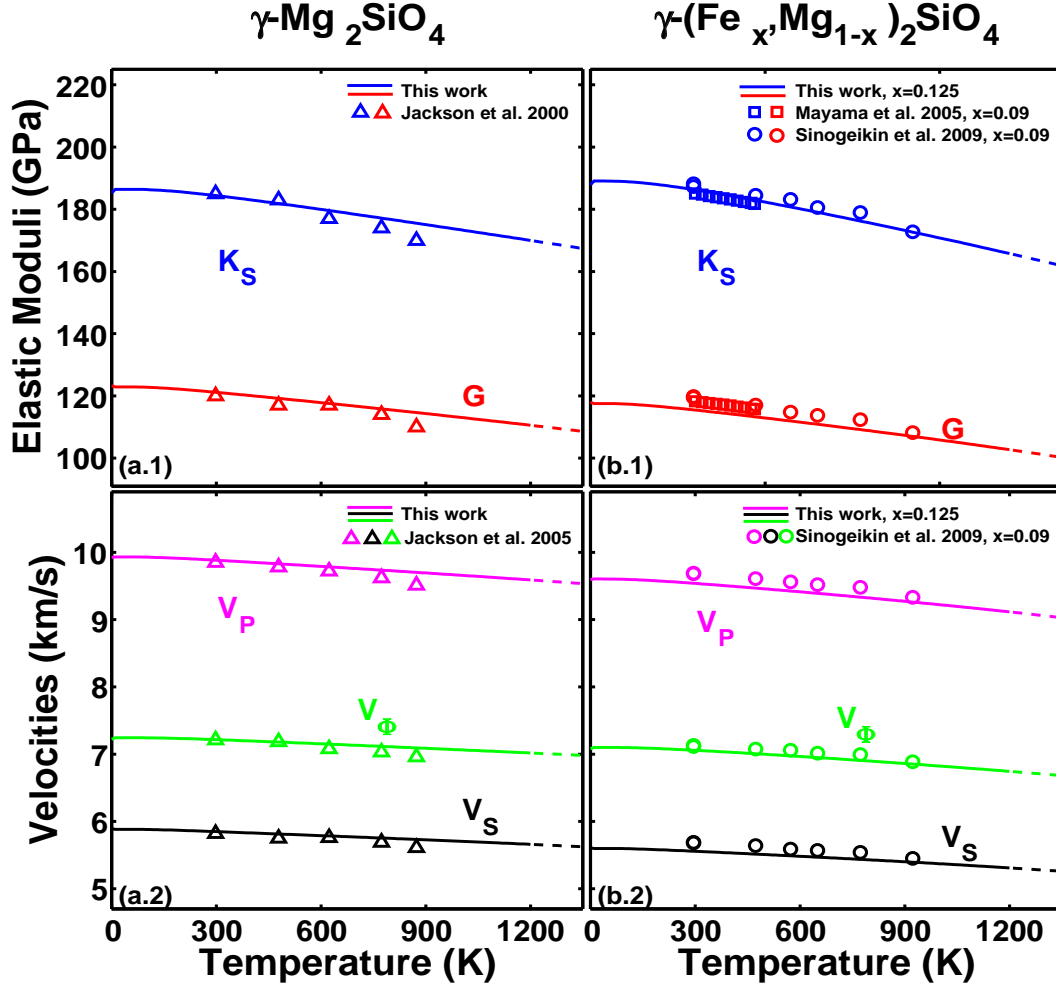


Figure 2: (Color online) Temperature dependence of bulk modulus (K), shear modulus (G), compressional velocity (V_P), shear velocity (V_S) and bulk velocity (V_Φ) for Mg-end member ringwoodite (a,c) and Fe-bearing ringwoodite (b,d). First principles calculations within LDA (solid lines) are compared to available experimental data (symbols) at $P=0$ GPa.

136 by these two factors.

137 The temperature dependence of elastic moduli and sound velocities of
138 Fe-free and Fe-bearing ringwoodite at ambient pressure are shown in Fig.
139 2. For $x = 0$, the agreement between experimental results (Jackson et al.,
140 2000) and our findings is outstanding (Figs. 2a and 2c). Similarly, our
141 predicted aggregate properties for $x = 0.125$ are in excellent correspondence
142 with experiments having $x = 0.09$ (Mayama et al., 2005; Sinogeikin et al.,
143 2003) (Figs. 2b and 2d). Predicted Fe-bearing K is larger than Fe-free K at
144 300 K (Table 1), and dK/dT is more negative for $x = 0.125$ than for $x = 0$.
145 On the other hand, G decreases with iron, but likewise K , dG/dT is more
146 negative for $x = 0.125$ than for $x = 0$. Predicted compressional, shear, and
147 bulk velocities as function of temperature are smaller than those reported
148 by Sinogeikin et al. (2003), which can be understood given the difference in
149 iron content (Fig. 2d). The x dependence of elastic moduli and velocities
150 for α -, β -, and γ -($\text{Fe}_x\text{Mg}_{1-x}$) $_2\text{SiO}_4$ at high temperatures and pressures
151 is shown in Fig. 3. We find dK/dx to be positive for all three phases,
152 while dG/dx , dV_P/dx , dV_S/dx , and dV_Φ/dx are negative. For small x , a
153 linear trend given by our results of elastic moduli and velocities compares
154 well to experimental data of olivine and ringwoodite. On the other hand,
155 experimental values of wadsleyite are more scattered and deviate the most
156 from the proposed linear behavior. Detailed dependence on pressure and
157 temperature of dK/dx , dG/dx , dV_P/dx , dV_S/dx , and dV_Φ/dx are shown in
158 Figs. 4 and 5. dK/dx and dG/dx for all three phases exhibit qualitatively
159 similar behavior in the pressure range considered. At low pressure they are
160 quite sensitive to temperatures, but they seem to converge at high pressure

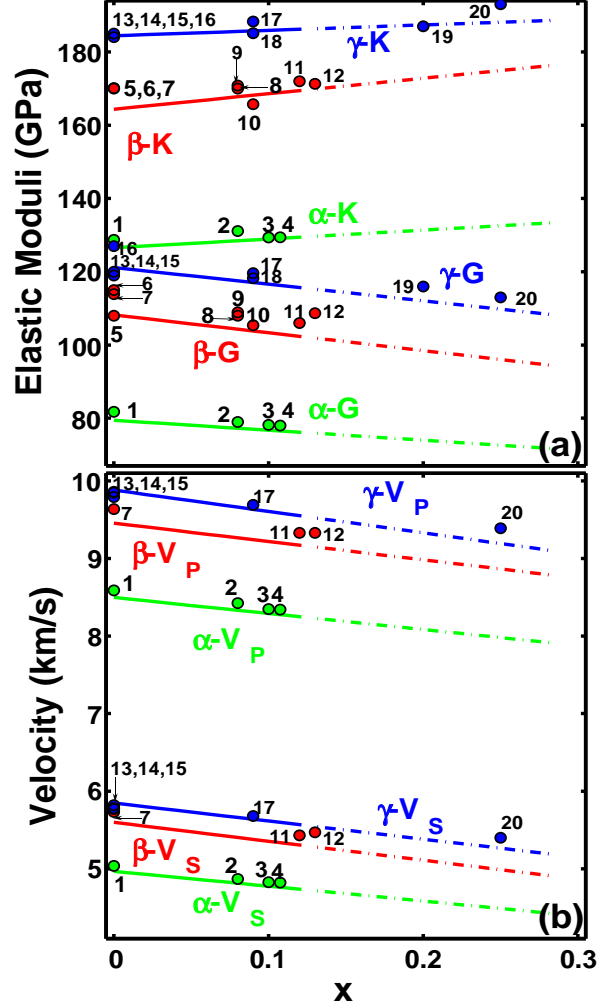


Figure 3: (Color online) Dependence on low iron content at $P = 0$ GPa and $T = 300$ K of a) elastic moduli, K and G , and b) velocities, V_P and V_S , (lines) compared to experimental data (circles): 1-Isaak et al. (1989); 2,3-Isaak (1992); 4-Abramson et al. (1997); 5-Li et al. (1996); 6-Zha et al. (1997); 7-Isaak et al. (2007); 8-Sinogeikin et al. (1998); 9-Isaak et al. (2010); 10-Mayama et al. (2004); 11-Li and Liebermann (2000); 12-Liu et al. (2009); 13-Weidner et al. (1984); 14-Jackson et al. (2000); 15-Li (2003); 16,19-Higo et al. (2006); 17-Sinogeikin et al. (2003); 18-Mayama et al. (2005); 20-Sinogeikin et al. (1997).

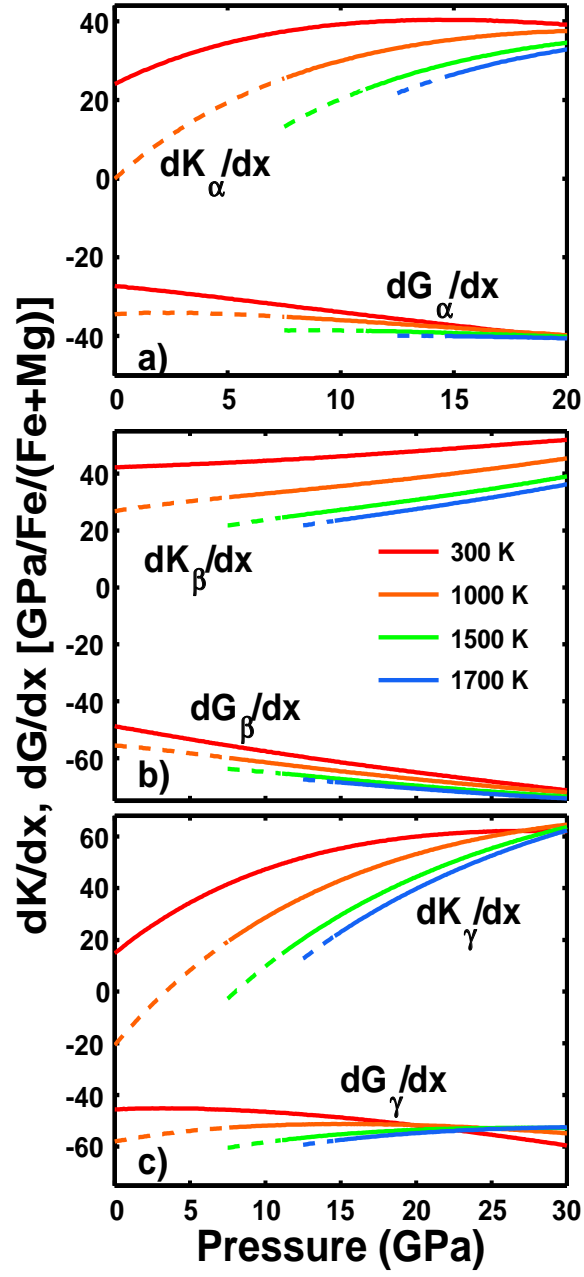


Figure 4: (Color online) Pressure dependence of dK/dx and dG/dx for a) olivine, b) wadsleyite, and c) ringwoodite.

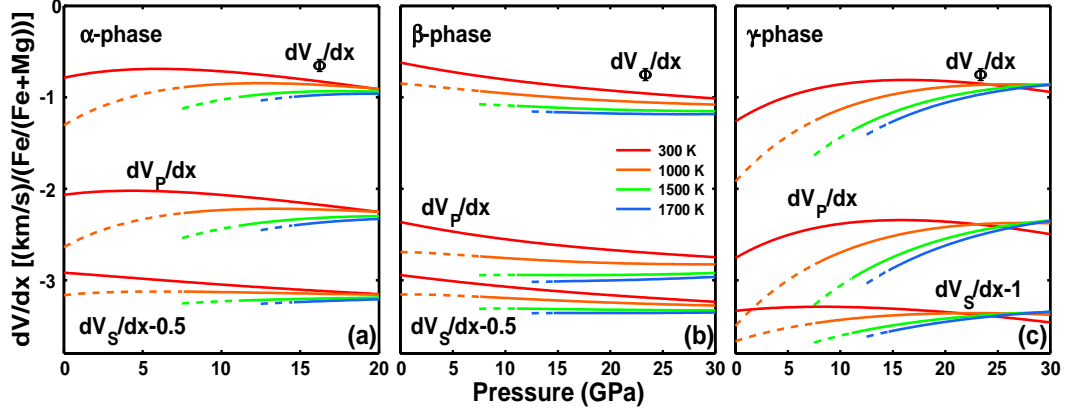


Figure 5: (Color online) Pressure dependence of dV/dx for a) olivine, b) wadsleyite, and c) ringwoodite.

161 (Figs. 4a and 4c). dV_P/dx , dV_S/dx , and dV_Φ/dx for all three phases are also
 162 more sensitive to temperature at lower pressures.

163 4. Geophysical implications: The 520 km Discontinuity

164 The seismic discontinuity near 520 km depth is often attributed to the
 165 phase change of wadsleyite to ringwoodite (Katsura and Ito, 1989; Shearer,
 166 1990; Revenaugh and Jordan, 1991). It is more likely to be unobserved than
 167 either of its near neighbors at 410-km and 660-km depth. It is, on average, a
 168 smaller amplitude feature (e.g. Revenaugh and Jordan, 1991) such that less
 169 frequent observation is to be expected. In some studies the 520 km disconti-
 170 nuity appears as a split arrival or doublet (e.g. Deuss and Woodhouse, 2001;
 171 Chambers et al., 2005; Bagley et al., 2009). When split, the two discontinu-
 172 ities are observed at depths of approximately 500 and 560 km (Deuss and Woodhouse,
 173 2001). Notably the sum of the two seismic features is larger than typical

174 non-split observations. Whether this is the result of an upward bias in iden-
 175 tifying split arrivals or the result of greater net velocity contrast it is not
 176 clear. Therefore accurate data on elasticity of wadsleyite and ringwoodite
 177 are critical for investigating the role of the transformation $\beta \rightarrow \gamma$ on the 520
 178 km seismic discontinuity. We use our results on aggregate properties of β -
 179 (Núñez Valdez et al., 2012) and γ -(Fe_x,Mg_{1-x})₂SiO₄ at temperatures and
 180 pressures encompassing the TZ to estimate the magnitude of the discontinu-
 181 ity across the phase transition. Although this is a divariant phase transition
 182 and calculation of the two-phase loop is beyond the scope of this work, we
 183 can clearly calculate velocity increases throughout the entire transition. As
 184 we saw in the previous section, experimental studies dealing with simultane-
 185 ous high pressures and temperatures offer limited data, and analyses usually
 186 extrapolate results at ambient conditions either in temperature or pressure
 187 to conditions near 520 km depth (~ 18 GPa and ~ 1600 K). The lack of other
 188 source of knowledge makes it difficult to outline conclusions and/or explain
 189 the nature of the 520 km seismic discontinuity. With this paper we hope to
 190 advance the understanding of this discontinuity.

191 To quantify the magnitude of the discontinuity across the β to γ transition
 192 at finite temperatures we use the contrast Δ of a particular property M
 193 defined as:

$$\Delta M = \frac{(M_{x,\gamma} - M_{x,\beta})}{\frac{(M_{x,\beta} + M_{x,\gamma})}{2}} \times 100, \quad (15)$$

194 where M could be density, elastic modulus, or velocity. Table 2 and Fig.
 195 6 show our calculated contrasts at finite temperatures for the $\beta \rightarrow \gamma$ tran-
 196 sition in Fe-free and Fe-bearing phases. We first notice that $\Delta\rho$ is almost
 197 independent of temperature and pressure with iron having an insignificant

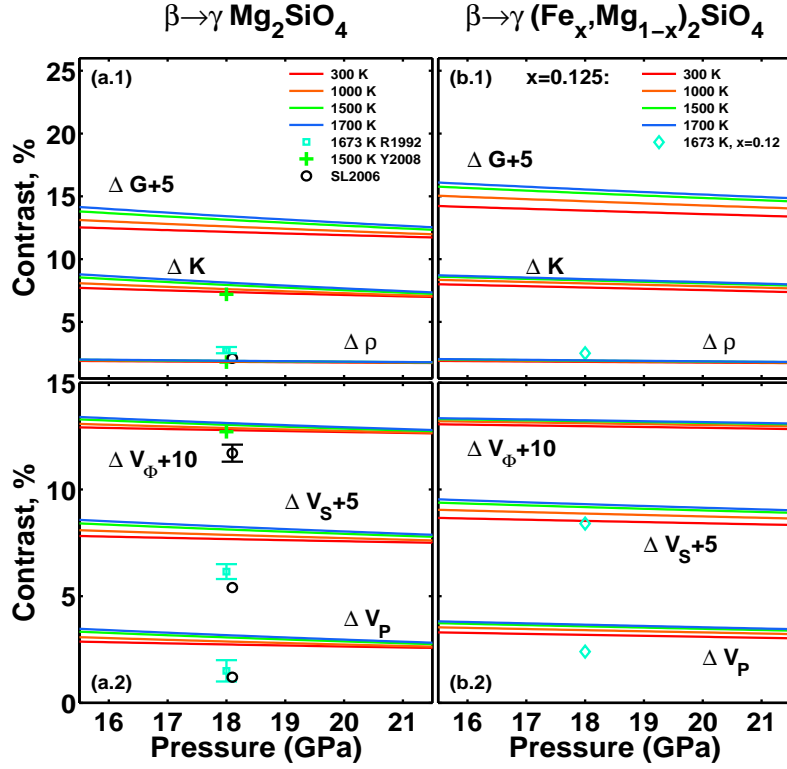


Figure 6: (Color online) Density, elastic, and velocity contrasts (lines) compared to laboratory and seismic data across the Fe-free (a,c) and Fe-bearing (b,d) $\beta \rightarrow \gamma$ transition. R1992: Rigden et al. (1992); Y2008: Yu et al. (2008); SL2006: Lawrence and Shearer (2006); $x = 0.12$: Sinogeikin et al. (2003).

198 effect (Figs. 6a and 6b), as suggested by Yu et al. (2008). Extrapolated
 199 experimental results and seismic data also suggested that iron should have
 200 a small effect on this quantity (Rigden et al., 1991; Lawrence and Shearer,
 201 2006; Sinogeikin et al., 2003). For $x = 0$ we obtain a very good agreement
 202 with a previous estimation by Yu et al. (2008). For $x = 0.125$ our result is
 203 slightly smaller than that by Sinogeikin et al. (2003) for $x = 0.09$. Contrasts
 204 of elastic moduli (Figs. 6a and 6b) indicate that ΔG is more sensitive to
 205 temperature than ΔK . This dependence is greater in $x = 0.125$ than in
 206 $x = 0$. In the 16–21 GPa range, both ΔG and ΔK slightly decrease with
 207 pressure, irrespective of x . Figs. 6c and 6d show that velocity contrasts,
 208 ΔV_P , ΔV_S , and ΔV_Φ , exhibit weak pressure dependence, decreasing only
 209 slightly with pressure. Temperature affects ΔV_S more than ΔV_P or ΔV_Φ .
 210 For $x = 0$, a comparison of our results to extrapolations of experimental
 211 data by Rigden et al. (1991) to 18 GPa and 1673 K and seismic data by
 212 Lawrence and Shearer (2006) shows predicted contrasts to be larger. ΔV_Φ is
 213 in better agreement with a previous prediction at 1700 K (Yu et al., 2008)
 214 and with a contrast from seismic studies (Lawrence and Shearer, 2006). Ve-
 215 locity contrasts increase with increasing x , however ΔV_S is the most enhanced
 216 by x , followed by ΔV_P , and ΔV_Φ . Extrapolations of ΔV_P and ΔV_S to 18 GPa
 217 and 1673 K with $x = 0.12$ reported by Sinogeikin et al. (2003) are smaller
 218 than our predicted contrasts, though ΔV_S is closer to our prediction.

219 In an attempt to explain the presence of two mid-transition zone disconti-
 220 nuities, Saikia et al. (2008) investigated the solubility of CaSiO_3 perovskite in
 221 majorite garnet at high-pressure (15–24 GPa) and high-temperature (1400°
 222 C–1600° C). They concluded that in fertile peridotite (i.e., peridotite en-

$\beta-(\text{Mg}_{1-x}\text{Fe}_x)_2\text{SiO}_4$				
V (\AA^3)	K (GPa)	G (GPa)	x	Reference
541.3	164.4	107.7	0	Núñez Valdez et al. (2012), Single crystal/DFT
-	170	108	0	Li et al. (1996), Poly-crystal/US
535.8(0.2)	170(2)	115(2)	0	Zha et al. (1997), Single crystal/BS
-	169.7(1.9)-170.7(2)	113.9(0.7)-114.1(0.8)	0	Isaak et al. (2007), Poly-crystal/RUS
541.5	169.5	101.7	0.125	This study, Single crystal/DFT
539.4(4)	170(3)	108(2)	0.08	Sinogeikin et al. (1998), Single crystal/BS
-	170.8(1.2)	108.9(0.4)	0.08	Isaak et al. (2010), Poly-crystal/RUS
-	165.72(6)	105.43(2)	0.09	Mayama et al. (2004), Poly-crystal/RUS
-	172(2)	106(1)	0.12	Li and Liebermann (2000), Poly-crystal/US
-	171.3(3)	108.7(2)	0.13	Liu et al. (2009), Poly-crystal/US
$\gamma-(\text{Mg}_{1-x}\text{Fe}_x)_2\text{SiO}_4$				
V (\AA^3)	K (GPa)	G (GPa)	x	Reference
527.6	184.4	120.95	0	This study, Single crystal/DFT
525.3	184	119	0	Weidner et al. (1984), Single crystal/BS
525.3	185(3)	120.4(2)	0	Jackson et al. (2000), Single crystal/BS
-	185(2)	120(1)	0	Li (2003), Poly-crystal/US
-	185(2)	127(1)	0	Higo et al. (2006), Poly-crystal/US
527.7	186.3	115.3	0.125	This study, Single crystal/DFT
526.2(4)	188.3(30)	119.6(20)	0.09	Sinogeikin et al. (2003), Single crystal/BS
-	185.11(0.16)-185.17(0.17)	118.27(0.06)	0.09	Mayama et al. (2005), Poly-crystal/RUS
-	187(2)	116(1)	0.20	Higo et al. (2006), Poly-crystal/US

Table 1: Results on wadsleyite and ringwoodite for volume (V), bulk (K), and shear (G), moduli at ambient pressure and temperature. US: Ultrasonic techniques; BS: Brillouin scattering techniques; RUS: Resonant Ultrasonic techniques.

223 riched in Ca and Al) at 1400° C, the wadsleyite to ringwoodite phase change
 224 produces a strong discontinuity at ~500–520 km depth, while the exsolution
 225 of Ca-perovskite produces a weak discontinuity near 540 km. At 1600° C, the
 226 two merge to form a single discontinuity at 540–560 km. In MORB-like com-
 227 positions, wadsleyite and ringwoodite are effectively absent, but exsolution
 228 of Ca-perovskite causes a velocity discontinuity near 560 km. Saikia et al.
 229 (2008) concluded that a mechanical mixture (or seismically averaged assem-
 230 blage) of peridotite and MORB would have two discontinuities: one near 500
 231 km due to the wadsleyite to ringwoodite phase change, and a second near
 232 560 km due to the exsolution of Ca-perovskite from garnet, consistent with
 233 a hypothesis of Deuss and Woodhouse (2001).

234 Of some question here is the association of the MORB-like mantle with
 235 the non-MORB component. If MORB is associated with peridotitic man-
 236 tle, the strength of the 500 km discontinuity would decrease with respect to
 237 that of the 520 km proportionally to the percentage of MORB. Since ΔV_S is
 238 smaller for the ex-solution of Ca-perovskite from majorite garnet in MORB-
 239 like material by a factor of 2 (Saikia et al., 2008), the summed strength of
 240 the two seismic discontinuities, at 500 km and 560 km, in a MORB plus
 241 peridotite mixture would be smaller than that of the 520 km alone. This
 242 is opposite to observations (Deuss and Woodhouse, 2001), and whether this
 243 is the result of an upward bias in identifying split arrivals or the result of
 244 greater net velocity contrast is not clear. If MORB is associated with MORB-
 245 depleted mantle (harzburgite or dunite) the greater wadsleyite fraction in the
 246 depleted mantle might compensate and increase in ΔV_S for the 500 km dis-
 247 continuity. However, the smaller fraction of iron in MORB-depleted mantle

T (K)	1500		1700	
x	0.0	0.125	0.0	0.125
$\Delta\rho$	1.89	1.92	1.91	1.94
ΔK	7.94	8.31	8.13	8.41
ΔG	8.14	10.26	8.42	10.55
ΔV_P	3.07	3.58	3.17	3.67
ΔV_S	3.12	4.17	3.26	4.31
ΔV_Φ	3.03	3.20	3.11	3.23
$\Delta(\rho V_P)$	4.96	4.99	5.08	5.11
$\Delta(\rho V_S)$	5.02	5.04	5.17	5.20

Table 2: Predicted contrasts in % across the $\beta \rightarrow \gamma$ -(Mg_{1-x},Fe_x)₂SiO₄ transition at 18 GPa.

(Jaques and Green, 1980) should decrease ΔV_S (as shown in Table 2) of the β to γ transition. The extent to which these effects counter-act each other and whether the greater summed strength of the two discontinuities can be explained by this picture, remains an open question.

5. Conclusions

For the first time, we have presented parameter-free first-principles results of high pressure and high temperature aggregate elastic properties and sound velocities of Fe-bearing ringwoodite. We used the QHA and a novel method of calculating elasticity at high temperatures (Wu and Wentzcovitch, 2011). Treatment of strain Grüneisen parameters via isotropic averages reduced greatly the computational cost of the task, which, otherwise, would have been

259 much more intensive and lengthy. Within the QHA limit, our predictions for
 260 elastic and acoustic properties for $x = 0$ were found to be in very good
 261 agreement with available experimental data at 300 K and ambient pressure
 262 (Li et al., 1996; Zha et al., 1997; Isaak et al., 2007; Li, 2003; Higo et al., 2006;
 263 Weidner et al., 1984) and molecular dynamics simulations (Li et al., 2006) at
 264 high pressures and temperatures. For $x = 0.125$ our results compared very
 265 well with experimental data in the range $x = 0.08 - 0.2$ (Sinogeikin et al.,
 266 1998; Li and Liebermann, 2000; Liu et al., 2009; Sinogeikin et al., 2003; Higo et al.,
 267 2006). High-temperature and ambient pressure results in ringwoodite also
 268 reproduced experimental trends very well (Isaak et al., 2007; Mayama et al.,
 269 2004; Isaak et al., 2010; Jackson et al., 2000; Mayama et al., 2005; Sinogeikin et al.,
 270 2003) for Fe-free and Fe-bearing samples.

271 Overall our predictions showed well defined changes in the elastic and
 272 acoustic properties of the β - and γ - phases near conditions of the 520 km
 273 seismic discontinuity. We show that pressure tends to decrease contrasts
 274 across the $\beta \rightarrow \gamma$ transition while temperature and iron concentration tend
 275 to enhance them. The absence of global observations of the 520 km discon-
 276 tinuity could suggest regions of the TZ with less iron and/or smaller olivine
 277 content and irregular temperature topography. Other considerations to try
 278 to explain the intermittent nature of the discontinuity would involve changes
 279 in the pyroxene/garnet/Ca-pv system and the amount of water present in the
 280 TZ. These issues will be addressed in future similar studies including other
 281 relevant phases.

282 6. Acknowledgments

283 Research supported by the NSF/EAR-1019853, and EAR-0810272. Com-
284 putations were performed using the VLab cyberinfrastructure at the Min-
285 nesota Supercomputing Institute.

286 References

- 287 Abramson, E.H., J. M. Brown, L. J. Slutsky, and J. Zaug, 1997. The elastic
288 constants of San Carlos olivine to 17 GPa, *Geophys. Res.*, 102, 12253–
289 12263.
- 290 Akaogi, M., E. Ito, and A. Navrotsky, 1989. Olivine-modified spinel-spinel
291 transitions in the system $\text{Mg}_2\text{SiO}_4\text{-Fe}_2\text{SiO}_4$: Calorimetric measurements,
292 thermochemical calculation, and geophysical application, *J. Geophys. Res.*,
293 94, 15 671–15 685.
- 294 Bagley, B., A. M. Courtier, and J. Revenaugh, 2009. Melting in the deep
295 upper mantle oceanward of the Honshu slab, *Physics of the Earth and*
296 *Planetary Interiors*, 175 (3-4), 137–144.
- 297 Baroni, S., A. Dal Corso, S. de Gironcoli, and P. Gianozzi, 2001. Phonons
298 and related crystal properties from density-functional perturbation theory,
299 *Rev. of Mod. Phys.*, 73(2), 515 LP–562 LP.
- 300 Carrier, P., R. M. Wentzcovitch, and J. Tsuchiya, 2007. First principles pre-
301 diction of crystal structures at high temperatures using the quasiharmonic
302 approximation, *Phys. Rev. B* 76, 064116.

303 Ceperley, D. M., and B. J. Alder, 1980. Ground state of the electron gas by
304 a stochastic method, *Phys. Rev. Lett.*, 45, pp. 566–569.

305 Chambers, K., A. Deuss, and J. Woodhouse, 2005. Reactivity of the 410-km
306 discontinuity from PP and SS precursors, *Journal of Geophysical Research*,
307 110 (B2), 1–13

308 Da Silveira, P., C. R. S. da Silva, and R. M. Wentzcovitch, 2008. Meta-
309 data management for distributed first principles calculations in VLab–A
310 collaborative cyberinfrastructure for materials computation, *Comp. Phys.*
311 *Comm.*, 178, 186.

312 Da Silveira, P., M. Nez Valdez, R. M. Wentzcovitch, M. Pierce, and D. A.
313 Yuen, 2011. VLab: an updated overview of system service and architecture,
314 *Proc. of Teragrid 2011 Conference*, in press.

315 Deuss, A., and J. Woodhouse 2001. Seismic observations of splitting of the
316 mid-transition zone discontinuity in Earths mantle., *Science*, 294 (5541),
317 354–7.

318 Giannozzi P. et al., 2009. QUANTUM ESPRESSO: a modular and open-
319 source software project for quantum simulations of materials, *J. Phys.:*
320 *Condens. Matter*, 21, 395502. <http://www.quantum-espresso.org>

321 Higo, Y., T. Inoue, B. Li, T. Irifune, and R. C. Liebermann, 2006. The effect
322 of iron on the elastic properties of ringwoodite at high pressure, *Phys.*
323 *Earth Planet. Inter.*, 159 pp. 276–285.

324 Hohenberg, P., and W. Kohn, 1964. Inhomogeneous Electron Gas, *Phys.*
325 *Rev.*, 136, B864–871.

326 Irifune, T., and A.E. Ringwood, 1987. Phase transformations in primitive
327 MORB and pyrolite compositions to 25 GPa and some geophysical impli-
328 cations, In: M. Manghnani and Y. Syono, Editors, High pressure Research
329 in Geophysics, TERRAPUB/AGU, Tokyo/Washington, D.C. (1987), pp.
330 231–242

331 Isaak, D. G., O. L. Anderson, T. Goto, and I. Suzuk, 1989. Elasticity of single-
332 crystal forsterite measured to 1700 K, *J. Geophys. Res.*, 94, 5895–5906.

333 Isaak, 1992. D. G. High-Temperature Elasticity of Iron-Bearing Olivines, *J.*
334 *Geophys. Res.*, 97, 1871–1885, 1992.

335 Isaak, D. G., G. D. Gwanmesia, D. Falde, M. G. Davis, R. S. Triplett, and l.
336 Wang, 2007. The elastic properties of β -Mg₂SiO₄ from 295 to 660 K and
337 implications on the composition of Earth’s upper mantle, *Phys. Earth and*
338 *Plan. Int.*, 162, 22–37.

339 Isaak, D. G., G. D. Gwanmesia, M. G. Davis, S. C. Stafford, A. M. Stafford,
340 and R. S. Triplett, 2010. The temperature dependence of the elasticity of
341 Fe-bearing wadsleyite, *Phys. Earth Planet. Int.*, 182, 107–112.

342 Jaques, A. L., and Green, D. H., 1980. Anhydrous melting of peridotite at
343 0–15 kb pressure and the genesis of tholeiitic basalts. *Contributions to*
344 *Mineralogy and Petrology*, 73, 287–310.

345 Jackson, J. M., S. V. Sinogeikin, and J. D. Bass, 2000. Sound velocities
346 and elastic properties of γ -(Mg₂SiO₄ to 873 K by Brillouin spectroscopy,
347 *Amer. Mineral.*, 85, 296–303.

348 Kohn, W., and L. J. Sham (1964), Self-Consistent equations including ex-
349 change and correlation effects, *Phys. Rev.*, 140, A1133–1138.

350 Katsura, T and E. Ito, 1989. The system $\text{Mg}_2\text{SiO}_4\text{-Fe}_2\text{SiO}_4$ at high pressures
351 and temperatures: Precise determination of stabilities of olivine, modified
352 spinel and spinel. *J. Geophys. Res.*, 94, 15 663–15 670.

353 Lawrence, J. F., P. M. Shearer, 2000. Constraining seismic velocity and den-
354 sity for the mantle transition zone with reflected and transmitted wave-
355 forms, *Geochem. Geophys. Geosyst.*, 7, Q10012.

356 Li, B., G. D. Gwanmesia, and R. C. Liebermann, 1996. Sound velocities
357 of Olivine and Beta Polymorphs of Mg_2SiO_4 at Earth’s Transition Zone
358 Pressures, *Geophys. Res. Lett.*, 23, 2259.

359 Li, B., and R. C. Liebermann, 2000. Sound velocities of wadsleyite
360 $\beta\text{-(Mg}_{0.88}\text{Fe}_{0.12})_2\text{SiO}_4$ to 10 GPa, *American Mineralogist*, 85, 292–295.

361 Li, B., 2003. Compressional and shear velocities of ringwoodite $\gamma\text{-(Mg}_2\text{SiO}_4$
362 to 12 GPa, *American Mineralogist*, 88, 1312–1317.

363 Li, L., D. J. Weidner, J. Brotholt, D. Alfè, and G. D. Price, 2006. Elasticity
364 of $(\text{Mg}_2\text{SiO}_4)$ ringwoodite at mantle conditions, *Phys. Earth Planet. Int.*,
365 157, 181–187.

366 Li, B., and R. C. Liebermann, 2007. Indoor seismology by probing the Earth’s
367 interior by using sound velocity measurements at high pressures and tem-
368 peratures, *Proceedings of the National Academy of Sciences*, 9145–9150.

369 Liu, W., J. Kung, B. Li, N. Nishiyma, and Y. Wang, 2009. Elasticity of
 370 β -(Mg_{0.87},Fe_{0.13})₂SiO₄ wadsleyite to 12 GPa and 1073 K, Phys. Earth
 371 Planet. Int., 174, 98–104.

372 Mayama, N., I. Suzuki, and T. Saito, 2004. Temperature dependence of elas-
 373 tic moduli of β -(Mg_{1-x},Fe_x)₂SiO₄, J. Geophys. Res., 31, L04612.

374 Mayama, N., I. Suzuki, T. Saito, I. Ohno, T. Katsura, and A. Yoneda, 2005.
 375 Temperature dependence of elastic moduli of ringwoodite, Phys. Earth
 376 Planet. Int., 148, 353–359.

377 Núñez Valdez, M., K. Umemoto, and R. M. Wentzcovitch, 2010. Funda-
 378 mentals of elasticity of (Mg_{1-x},Fe_x)₂SiO₄-olivine, Geophys. Res. Lett., 37,
 379 L14308.

380 Núñez Valdez, M., P. da Silveira, and R. M. Wentzcovitch, 2011. Influence of
 381 Iron on the Elastic Properties of Wadsleyite and Ringwoodite, J. Geophys.
 382 Res., 116, B12207.

383 Núñez Valdez, Z. Wu, Y. G. Yu and R. M. Wentzcovitch, 2012. Thermoe-
 384 lastic Properties of Olivine and Wadsleyite (Mg_{1-x},Fe_x)₂SiO₄: Their Rela-
 385 tionship to the 410 km Seismic Discontinuity, Geophys. Res. Lett., under
 386 review.

387 Putnis, A., 1992. Introduction to Mineral Sciences, 399 pp., Cambridge Uni-
 388 versity Press, UK

389 Revenaugh, J., T.H. Jordan, 1991. Mantle layering from ScS reverberations.
 390 2. The Transition zone, J. Geophys. Res., 96, 19,763–19,780.

391 Rigden, S.M., G. D. Gwanmesia, J. D. Fitz Gerald, I. Jackson, and R. C.
392 Liebermann, 1991. Spinel elasticity and seismic structure of the transition
393 zone of the mantle, *Nature*, 354, 143–145.

394 Rigden, S.M., G. D. Gwanmesia, I. Jackson, and R. C. Liebermann, 1992.
395 Progress in high-pressure dependence of elasticity of Mg_2SiO_4 polymorphs
396 and constraints on the composition of the transition zone of the Earth’s
397 mantle. In: Syono, Y., Manghnani, M.H. (Eds.), *High-Pressure Research:*
398 *Application to Earth and Planetary Science*. Geophys. Monogr. Ser. 67,
399 Am. Geophys. Union, 167–182

400 Rinwood, A.E., 1975. Composition and petrology of the Earth’s mantle, 618
401 pp., McGraw-Hill, New York

402 Saikia, A., D. J. Frost, and D. C. Rubie (2008). Splitting of the 520-kilometer
403 seismic discontinuity and chemical heterogeneity in the mantle, *Science*,
404 319(5869), 1515–1518.

405 Shearer, P. M. (1990). Seismic imaging of upper-mantle structure with new
406 evidence for a 520-km discontinuity, *Nature*, 344 (6262), 121–126.

407 Sinogeikin, S. V., J. D. Bass, A. Kavner, and R. Jeanloz, 1997. Elasticity of
408 natural majorite and ringwoodite from the Catherwood meteorite, *Geophys. Res. Lett.*, 24(24), 3265–3268.

410 Sinogeikin, S. V., T. Katsura, and J. D. Bass, 1998. Sound velocities and
411 elastic properties of Fe-bearing wadsleyite and ringwoodite, *J. Geophys.*
412 *Res.*, 103(B9), 20,819–20,825.

413 Sinogeikin, S. V., J. D. Bass, and T. Katsura, 2003. Single-crystal elasticity
414 of ringwoodite to high pressures and high temperatures: implications for
415 520 km seismic discontinuity, *Phys. Earth Planet. Inter.*, 136, 41–66.

416 Stackhouse, S., L. Stixrude, B. B. Karki, 2010. Determination of the high-
417 pressure properties of fayalite from first-principles calculations, *Earth and*
418 *Planet. Sc. Lett.* 289, 449–456.

419 Vanderbilt, D., 1990. Soft self-consistent pseudopotentials in a generalized
420 eigenvalue formalism, *Phys. Rev. B*, 41, R7892.

421 Wallace, D. C., 1972. *Thermodynamics of Crystals*, John Wiley & Sons, Inc.,
422 USA.

423 Watt, J. P., G. F. Davies, and R. J. O’Connell, 1976. The Elastic Properties
424 of Composite Materials, *Rev. of Geoph. and Spac. Phys.*, 50, 6290–6295.

425 Watt, J. P., 1979. Hashin-Shtrikman bounds on the effective elastic moduli of
426 polycrystals with orthorhombic symmetry, *J. Appl. Phys.*, 50, 6290–6295.

427 Weidner, D. J., H. Sawamoto, S. Sasaki, and M. Kumazawa, 1984. Single-
428 crystal elastic properties of the spinel phase of Mg_2SiO_4 , *J. Geophys. Res.*,
429 89(B9), 7852–7860.

430 Wentzcovitch, R. M., 1991. Invariant molecular dynamics approach to struc-
431 tural phase transitions, *Phys. Rev. B*, 44, 2358–2361.

432 Wentzcovitch, R. M., J. L. Martins, and G. D. Price, 1993. *Ab initio* molec-
433 ular dynamics with variable cell shape: application to MgSiO_3 perovskite,
434 *Phys. Rev. Lett.*, 70, 3947–3950.

- 435 Wu, Z. and Wentzcovitch R. M., 2011. Quasiharmonic thermal elasticity of
436 crystals: An analytical approach. Phys. Rev. B 83, 184115
- 437 Y. Yu, Z. Wu, and R. M., Wentzcovitch, 2008. $\alpha \leftrightarrow \beta \leftrightarrow \gamma$ transformations in
438 Mg_2SiO_4 in Earth's transition zone, Earth Planet. Sci. Lett., 273, 115-122.
- 439 Zha, C.S., T.S. Duffy, H.W. Mao, R.T. Downs, R.J. Hemley and D.J. Weid-
440 ner, 1997), Single-crystal elasticity of $\beta\text{-Mg}_2\text{SiO}_4$ to the pressure of the 410
441 km seismic discontinuity in the earth's mantle, Earth Planet. Sci. Lett.,
442 147, E9–E15